

# Interpreting a CMS $lljj\cancel{p}_T$ Excess With the Golden Cascade of the MSSM

Ben Allanach,<sup>1</sup> Anders Kvellestad,<sup>2</sup> and Are Raklev<sup>1,2</sup>

<sup>1</sup>DAMTP, CMS, Wilberforce Road, University of Cambridge, Cambridge, CB3 0WA, United Kingdom

<sup>2</sup>Department of Physics, University of Oslo, N-0316 Oslo, Norway

The CMS experiment recently reported an excess consistent with an invariant mass edge in opposite-sign same flavor (OSSF) leptons, when produced in conjunction with at least two jets and missing transverse momentum. We provide an interpretation of the edge in terms of (anti-)squark pair production followed by the ‘golden cascade’ decay for one of the squarks:  $\tilde{q} \rightarrow \tilde{\chi}_2^0 q \rightarrow \tilde{l} l q \rightarrow \tilde{\chi}_1^0 q l l$  in the minimal supersymmetric standard model (MSSM). A simplified model involving binos, winos, an on-shell slepton, and the first two generations of squarks fits the event rate and the invariant mass edge. We check consistency with a recent ATLAS search in a similar region, finding that much of the good-fit parameter space is still allowed at the 95% confidence level (CL). However, a combination of other LHC searches, notably two-lepton stop pair searches and jets plus  $\cancel{p}_T$ , rule out all of the remaining parameter space at the 95% CL.

PACS numbers: 12.60.Jy, 13.15.tg, 14.80.Ly

## I. INTRODUCTION

A recent CMS search for beyond the standard model physics in a channel with at least two leptons, at least two jets and missing transverse momentum ( $\cancel{p}_T$ ), reports a  $2.6\sigma$  excess [1] for  $19.4 \text{ fb}^{-1}$  of integrated luminosity at a centre of mass energy of 8 TeV.<sup>1</sup> The signal consists of two isolated OSSF leptons  $l$  ( $e$  or  $\mu$ ).  $e\mu$  opposite sign opposite-flavor (OSOF) leptons are used to measure the backgrounds accurately. These are dominated by  $t\bar{t}$  production, which gives equal rates for the same-flavor and opposite-flavor channels. Drell-Yan production of  $\gamma^*/Z^0$  bosons is a secondary irreducible background, yielding same-flavor events, and is estimated by a control region in the event kinematics which does not overlap with the signal region. The ATLAS experiment has looked in a similar signal region as CMS [3], and seen no excess, and so the two experimental results appear at first sight to be in tension with one another.

The CMS excess over the Standard Model expectation is depicted in Fig. 1 and shows an interesting kinematical feature: the invariant mass of the lepton pair  $m_{ll}$  is consistent with a right triangular shaped kinematic edge at  $m_{ll} = 78.7 \pm 1.4 \text{ GeV}$  [1]. Features such as edges are less likely to come from mis-modelling the detector response to backgrounds than smoother shapes, and so they are particularly welcome as indicators of a signal. This triangular edge is a classic signal of the production of supersymmetric (SUSY) particles which undergo two-body cascade decays through successively lighter on-shell SUSY particles, for example the chain  $\tilde{\chi}_2^0 \rightarrow \tilde{l}^- l^+ \rightarrow \tilde{\chi}_1^0 l^- l^+$ . The jets in the signal events could either be the result of initial state radiation, or of the  $\tilde{\chi}_2^0$  being produced itself by the decay of a squark  $\tilde{q} \rightarrow \tilde{\chi}_2^0 q$ .

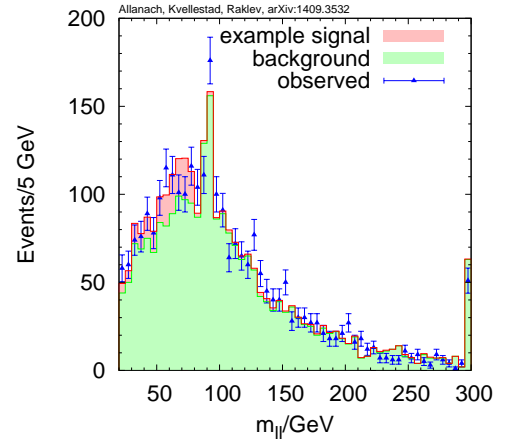


FIG. 1. Invariant mass distribution of OSSF leptons in the CMS selection after cuts. The expected Standard Model background is shown (green), which is calculated from data by using OSOF events, as well as the observed data and an example signal point (red) in the parameter space investigated here involving the golden cascade:  $m_{\tilde{q}} = 900 \text{ GeV}$ ,  $m_{\tilde{\chi}_2^0} = 312 \text{ GeV}$ ,  $m_{\tilde{l}_R} = 200 \text{ GeV}$ ,  $m_{\tilde{\chi}_1^0} = 216 \text{ GeV}$ . Error bars on the observed number of events show the expected statistical standard deviation.

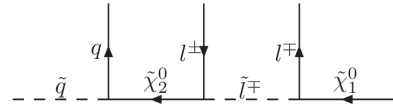


FIG. 2. Feynman diagram for the golden cascade decay.

This golden chain, starting from the squark, see Fig. 2, has been intensely studied for the possibilities it brings for determining the parameters of the sparticles involved, such as mass and spin. For a review see [4].

The MSSM predicts that the LHC produces pairs of SUSY particles, *e.g.* squarks and neutralinos, each with

<sup>1</sup> After the initial completion of this paper the CMS experiment published a more complete account of the results of that search in [2].

various possible decay chains. As an interpretation of the excess CMS gave three benchmark model points with a sbottom squark in the cascade decay chain [1].<sup>2</sup> They showed that the predicted  $m_{ll}^{max}$  distribution was roughly in agreement with data for two of their benchmarks but provided no scan of the parameter space or other tests of the benchmarks. Production from sbottoms was investigated further in [7].

Here, we shall instead interpret the excess in terms of the production of squarks from the first two generations, and provide a more comprehensive exploration of the interesting parameter space in Sec. II. The null results of the corresponding ATLAS search and strong direct constraints on light flavoured squarks from LHC searches for jets and  $\cancel{p}_T$  and no leptons, will have an impact on the allowed parameter space. In Sec. III we shall investigate whether the interpretation of this CMS excess involving the golden channel is consistent with these and other collider constraints. Finally, we draw our conclusions in Sec. IV.

## II. PARAMETER SPACE FITTING THE CMS EXCESS

The edge in  $m_{ll}$  predicted by the  $\tilde{\chi}_2^0$  decay chain is due to kinematics: one finds [8], by energy-momentum conservation, that in the decay chain described above with an on-shell slepton  $\tilde{l}$ , it has a maximum value

$$m_{ll}^{max} = \sqrt{\frac{(m_{\tilde{\chi}_2^0}^2 - m_{\tilde{l}}^2)(m_{\tilde{l}}^2 - m_{\tilde{\chi}_1^0}^2)}{m_{\tilde{l}}^2}}. \quad (1)$$

Thus, measurement of the edge leads to a constraint upon the masses of the three SUSY particles involved in the decay.

We show the edge constraint on the masses coming from the central value inferred from CMS data in Fig. 3. From the endpoint constraint alone the hyper-surface will extend to infinite masses, while from below it only bounds the mass of  $\tilde{\chi}_2^0$ . The errors on the CMS fit to the edge are so small that varying  $m_{ll}^{max}$  within them would produce no visible difference in the figure.

In our interpretation we follow the CMS counting experiment analysis where two OSSF leptons are required to have transverse momentum  $p_T > 20$  GeV and pseudorapidity  $|\eta| < 2.4$ , excluding the range  $1.4 < |\eta| < 1.6$  where electron and muon efficiencies differ greatly. Jets are reconstructed by the anti- $k_T$  algorithm [9] using FastJet [10], with a jet radius parameter of  $R = 0.5$ , and are required to have  $p_T > 40$  GeV and lie within  $|\eta| < 3.0$ . A combination of two jets and missing transverse momentum  $\cancel{p}_T > 150$  GeV, or three or more jets and  $\cancel{p}_T > 100$

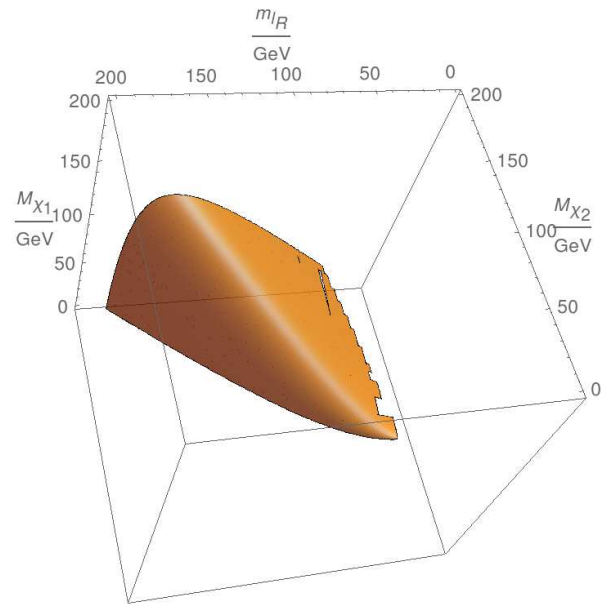


FIG. 3. Constraint on SUSY particle masses involved in the  $\tilde{\chi}_2^0$  decay coming from the central value  $m_{ll}^{max} = 78.7$  GeV.

GeV, is required in the events. For di-lepton invariant masses in the range  $20 \text{ GeV} < m_{ll} < 70 \text{ GeV}$  the total CMS background estimate is  $730 \pm 40$  events for central production (both leptons within  $|\eta| < 1.4$ ), whereas 860 OSSF were observed, corresponding to a  $2.6\sigma$  deviation. The deviation of  $130^{+48}_{-49}$  events constrains the MSSM parameter space.

For given  $m_{\tilde{\chi}_1^0}$  and  $m_{\tilde{\chi}_2^0}$  masses and the measured  $m_{ll}^{max}$ , there are at most two possible positive real solutions of Eq. (1) for  $m_{\tilde{l}}$ . In the rest of this work we shall pick  $m_{\tilde{l}}$  and either  $m_{\tilde{\chi}_1^0}$  or  $m_{\tilde{\chi}_2^0}$  by changing an input parameter, then impose Eq. (1) by solving it for the other neutralino mass. Then, the overall interpreted signal rate gives the mass for the squarks: the heavier they are, the smaller the production cross section and the smaller the rate.

We shall use a bottom-up prescription in order to fit the CMS excess, setting MSSM particles that are irrelevant for the signal to be heavy. We use as free parameters the wino soft-mass  $M_2$ , a common first and second generation<sup>3</sup> right-handed soft mass  $m_{\tilde{l}_R}$ , solving for the correct value of the bino soft-mass  $M_1$ ,<sup>4</sup> and a common first and second generation squark mass (both left- and right-handed)  $m_{\tilde{q}}$ . The mass of the SUSY partner of the left-handed lepton  $m_{\tilde{l}_L}$  is fixed to be  $2m_{\tilde{l}_R}$ . Setting

<sup>2</sup> In this chain, the  $\tilde{\chi}_2^0$  decays through an off-shell  $Z$ , which does not predict an exact triangular di-lepton distribution [5, 6].

<sup>3</sup> CMS did not release a flavor decomposition of the events. Given more statistics, this can be used to infer a possible smuon-selectron mass splitting [11].

<sup>4</sup> We consider both hierarchies:  $M_2 > M_1$  (bino dominated LSP) and  $M_2 < M_1$  (wino dominated LSP). Higgsinos only couple extremely weakly to selectrons or smuons and so would result in rates that were far too small if they were involved in the chain.

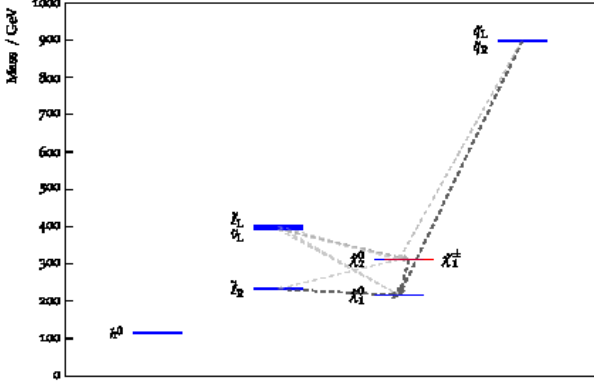


FIG. 4. Example signal point that fits the edge inference:  $m_{\tilde{q}} = 900$  GeV,  $m_{\tilde{\chi}_2^0} = 312$  GeV,  $m_{\tilde{t}_R} = 200$  GeV,  $m_{\tilde{\chi}_1^0} = 216$  GeV. Prominent decays with branching ratios higher than 10% are shown as arrows.

$m_{\tilde{t}_L} < m_{\tilde{\chi}_2^0}$  would introduce the  $\tilde{t}_L$  into the decay chain, as well as light sneutrinos that steal branching ratio from the golden cascade, and thus lower the signal rate.

Except the gluino mass, which is set to 1.6 TeV, all other soft masses are decoupled at <sup>5</sup> 3500 GeV, and the trilinear soft SUSY breaking scalar couplings are set to zero. Decoupling the gluino mass makes it easier for the scenario to pass constraints from searches in the jets plus  $\cancel{p}_T$  channel, however, an alternative interpretation could potentially be found by decoupling the squarks instead. We also set  $\tan\beta = 10$ . Although this is a parameter in the neutralino mass matrix we have checked that changing  $\tan\beta$  has a negligible effect on our CMS fit. We show an example spectrum, along with prominent decays, in Fig. 4.

We calculate the resulting sparticle spectrum using SOFTSUSY 3.5.1 [13] and the sparticle branching ratios with SUSYHIT 1.4 [14]. Spectrum and decay information is communicated via the SUSY Les Houches Accord [12]. For given values of  $m_{\tilde{t}_R}$  and  $M_2$ ,  $M_1$  is calculated to solve Eq. (1).

We calculate the production cross-section of squarks and anti-squarks to next-to-leading order for these parameter points using a fit to results from Prospino [15]. Figure 5 shows the prediction for the production cross-section of (anti-)squarks at an 8 TeV LHC. We have fitted a function such that

$$\log_{10} \sigma/\text{fb} = a_2 x^2 + a_1 x + a_0, \quad (2)$$

where  $x = m_{\tilde{q}}(M_{SUSY})/(1 \text{ TeV})$  is proportional to the squark mass input parameter. The squark mass input depends upon the modified  $\overline{DR}$  mass renormalisation scale,

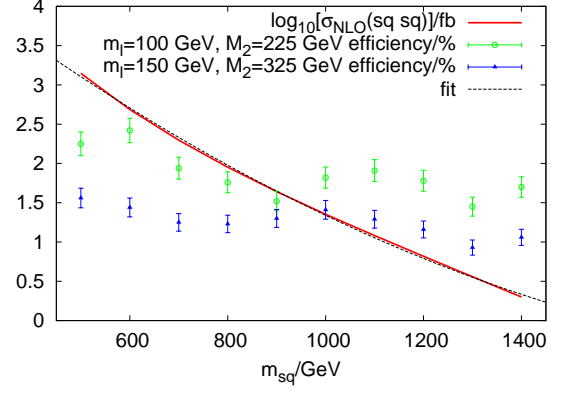


FIG. 5. Fit to (anti-)squark production cross-section at an 8 TeV LHC. The logarithm of the Prospino cross-section prediction is shown by the solid line. Our quadratic fit to this is shown by the dashed line. The CMS  $lljj\cancel{p}_T$  search region cut efficiencies for example parameter space points are shown by the points with errorbars, where the errorbars are purely from Monte Carlo statistics.

which we have set equal to the geometric mean of the two stop masses ( $M_{SUSY}$ ). Our fit yields  $a_2 = 1.12855$ ,  $a_1 = -5.22317$  and  $a_0 = 5.43447$ . The production cross-section varies rapidly with squark mass: in the mass region checked, a factor of 3 in squark mass results in 3 orders of magnitude reduction in the (anti-)squark production cross-section.

We then generate 40 000 SUSY Monte Carlo events per parameter point using Pythia 8.186 [16, 17]. These events are propagated through our implementation of the CMS analysis. Figure 5 shows that the efficiency of the cuts of the CMS  $lljj\cancel{p}_T$  signal region (see below) varies much more slowly with squark mass input parameter than the cross section. This suggests a strategy for finding the correct squark mass to yield a desired signal yield: we first calculate the number of expected events in the CMS signal region for an initial input squark mass parameter (we take 1000 GeV). Then we calculate  $\sigma$  needed for our desired signal yield, assuming that the efficiency does not change. We solve Eq. (2) for  $x$ , set the squark mass input parameter to  $x \times 1 \text{ TeV}$ , then calculate the cut efficiency from the sample of simulated signal events. This process is iterated until the squark mass converges, allowing us to efficiently find points in the three-dimensional  $m_{\tilde{t}_R}$ ,  $\Delta m = M_2 - m_{\tilde{t}_R}$ ,  $m_{\tilde{q}}(M_{SUSY})$  input parameter space that correspond to a given number of CMS  $lljj\cancel{p}_T$  signal region events. Convergence here is defined as the input squark mass changing by less than 10 GeV between the previous iteration and the present.

The predicted  $m_{ll}$  distribution of an example point that fits the inferred edge along with the rate is shown in Fig. 1. It is consistent with the CMS  $lljj\cancel{p}_T$  data. However, we shall eventually show that a combination of constraints will rule out the golden channel interpretation of the excess to 95% CL. In order to make this interpreta-

<sup>5</sup> Instead of fixing the Lagrangian parameters for the soft SUSY breaking Higgs mass parameters, we calculate them by minimising the MSSM Higgs potential after fixing  $M_A$  and the  $\mu$  parameter to 3500 GeV [12].

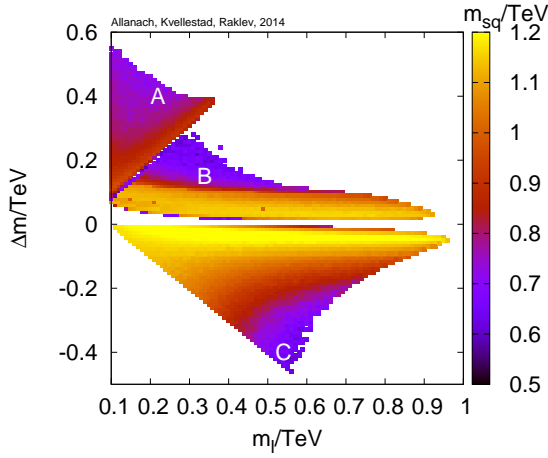


FIG. 6. Constraints on golden channel parameter space from the CMS  $lljj\cancel{p}_T$  search over the input parameter plane  $m_{\tilde{l}}(M_{SUSY})$  and  $\Delta m = M_2(M_{SUSY}) - m_{\tilde{l}}(M_{SUSY})$ . A coloured box indicates a point that fits the 95% CL lower limit of the inferred value of CMS  $lljj\cancel{p}_T$  signal rate and is also consistent with CMS's edge inference.

tion robust, we wish to show that even CMS  $lljj\cancel{p}_T$  signal rates at the 95% lower boundary are excluded: higher signal rates would result from higher production cross-sections, *i.e.* lower squark masses, but this would then produce higher rates for the other searches, disfavouring the golden channel interpretation even more. Profiling over Gaussian background uncertainties, the observation of 860 events in the signal region over a background of  $730 \pm 40$  yields a 95% CL lower limit of 34 signal events. We will therefore find the parameter space corresponding to this number of predicted signal events.

In Fig. 6 we show the region of input parameter space that fits the CMS  $lljj\cancel{p}_T$  signal rates at the 95% lower boundary. Wherever a coloured point is plotted, there is a viable solution. Blank regions of the plot either require squark masses that are below 500 GeV in order to get high enough signal rates, or do not contribute to the signal because decays do not give the required topology. For  $\Delta m < 0$ , the LSP is wino-dominated, whereas for  $\Delta m > 0$ , it is bino-dominated. We see that the two signs of  $\Delta m$  are separated by a region where the resulting leptons tend to be too soft to give appreciable signal rates. The colour of the point gives the physical average light squark mass by reference to the colour bar on the right-hand side. Squark masses up to 1200 GeV are predicted, depending upon parameters. We have divided the parameter space up into three connected regions: A, B and C as shown on the figure. We show the main decay modes relevant to the golden channel for each region in Table I.

The location of region A, and in particular the slope dividing it from region B, of course depends on the relationship  $m_{\tilde{l}_L} = 2m_{\tilde{l}_R}$  that we have fixed. However, the exact value of that slope will have little effect on the following discussion as long as  $m_{\tilde{l}_L} > m_{\tilde{l}_R}$ . In region C,

Region	mode
A	$\tilde{q}_L \rightarrow q\tilde{\chi}_2^0 \rightarrow q\tilde{l}_L l \rightarrow ql^+l^-\tilde{\chi}_1^0$ $\tilde{q}_R \rightarrow q\tilde{\chi}_1^0$
B	$\tilde{q}_L \rightarrow q\tilde{\chi}_2^0 \rightarrow q\tilde{l}_R l \rightarrow ql^+l^-\tilde{\chi}_1^0$ $\tilde{q}_R \rightarrow q\tilde{\chi}_1^0$
C	$\tilde{q}_R \rightarrow q\tilde{\chi}_2^0 \rightarrow q\tilde{l}_R l \rightarrow ql^+l^-\tilde{\chi}_1^0$ $\tilde{q}_L \rightarrow q\tilde{\chi}_1^0$

TABLE I. Main relevant decay modes of each connected region in Fig. 6.

where  $\Delta m < 0$ , the LSP is wino-dominated and so there is a sizeable branching fraction for squarks to decay via the lightest charginos instead.

Figure 7 displays the same points plotted as functions of the physical masses of the second-lightest neutralinos and the right-handed sleptons. In the upper panel, we display the physical squark mass that fits the 95% CL lower inferred rate and in the lower panel, the lightest neutralino mass as inferred from the edge constraint in Eq. (1). There is an upper bound on slepton masses  $m_{\tilde{l}_R} < 1000$  GeV implied by the fit. This is because in order to get a sizeable decay rate for the golden cascade, we require the mass ordering  $m_{\tilde{q}} > m_{\tilde{\chi}_2^0} > m_{\tilde{l}_R} > m_{\tilde{\chi}_1^0}$  and for such high  $m_{\tilde{q}}$ , it is no longer possible to get a large enough signal event rate.  $m_{\tilde{\chi}_1^0}$  is highly correlated with  $m_{\tilde{l}_R}$  in order to get the central inferred  $m_{\tilde{l}_R}^{\max}$  value, and lies in the range 50 GeV to 800 GeV. In the upper panel, we label where the regions A, B or C are mapped to on the physical mass plane. In fact, region C is mapped to a small region close to the ‘No golden channel line’ on top of region B in the physical mass plane where  $\tilde{\chi}_2^0$  and  $\tilde{l}_R$  are virtually degenerate.

### III. CONSTRAINTS FROM OTHER SEARCHES

Both ATLAS [18] and CMS [19] have searched in the jets and  $\cancel{p}_T$  channel. Neither experiment observed a significant excess, and the exclusions from each are rather similar. Here, we constrain our parameter space with an ATLAS search at 8 TeV in  $20.3 \text{ fb}^{-1}$  of integrated luminosity [18] in the ‘3j’ signal region. This signal region is chosen to be efficient for the type of events with a low number of high- $p_T$  jets expected from the topologies in Table I.

Any events with isolated muons or electrons are vetoed, and ATLAS requires  $\cancel{p}_T > 160$  GeV, and the three hardest anti- $k_T$  jets with  $|\eta| < 2.5$  and  $R = 0.4$  to have at least 130 GeV, 60 GeV and 60 GeV, respectively. Their azimuthal angle must differ from that of the reconstructed  $\cancel{p}_T$  by  $\Delta\phi > 0.4$ . Defining the effective mass  $m_{eff}$  as the scalar sum of  $\cancel{p}_T$  and the  $p_T$  of the hardest three jets, the cuts  $\cancel{p}_T/m_{eff} > 0.3$  and  $m_{eff} > 2200$  are also imposed. ATLAS observed 7 events on a background of  $5.0 \pm 1.2$ , from which they deduce an upper bound of



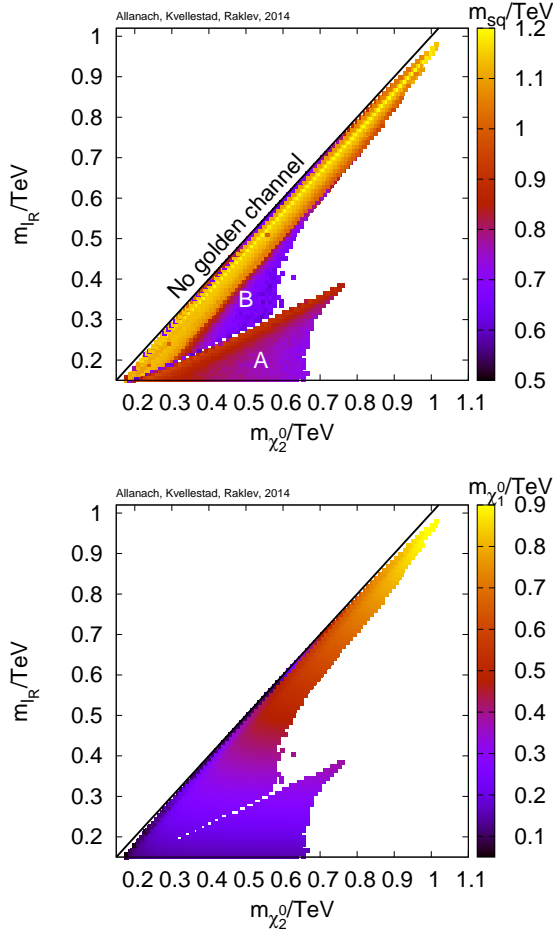


FIG. 7. Constraints on golden channel parameter space from the CMS  $lljj\cancel{p}_T$  search over the plane of pole masses of the second-lightest neutralino and the right-handed slepton. A coloured box indicates a point that fits the 95% CL lower limit of the inferred value of CMS  $lljj\cancel{p}_T$  signal rate and is also consistent with CMS's edge inference. The squark mass (upper panel) or lightest neutralino mass (lower panel) is given by reference to the scale on the right-hand side. Above the black line, the golden channel is kinematically inaccessible.

8.2 signal events to 95% CL. We impose this constraint upon our expected signal yields, having checked that our implementation of the analysis is consistent with ATLAS results in terms of cut-flow.

Figure 8 shows that a large fraction of otherwise viable parameter space is excluded by the jets plus  $\cancel{p}_T$  constraint, but that a portion of parameter space with  $m_{\tilde{l}} > 400$  GeV survives the constraint, despite having squark masses as low as 750 GeV. The potency of the jets plus  $\cancel{p}_T$  search is reduced by the large leptonic branching ratio in this region of the plot, and lower signal rates due to the fact that we have set the gluino mass to be rather high at 1.6 TeV.<sup>6</sup>

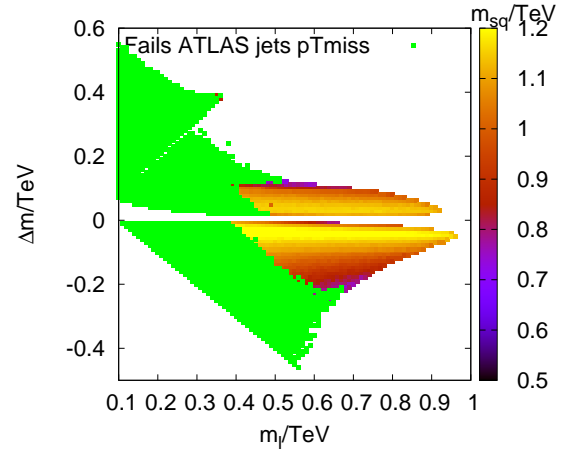


FIG. 8. Constraints on golden channel parameter space from the ATLAS jets plus  $\cancel{p}_T$  search. The squark mass consistent with the 95% CL lower bound on the CMS  $lljj\cancel{p}_T$  signal is given by reference to the scale on the right-hand side. Points coloured green are excluded by an ATLAS  $\cancel{p}_T$  plus jets search at the 95% CL.

Since CMS published its  $2.6\sigma$  excess, ATLAS has checked a similar signal region, which they call the ‘off- $Z$ ’ region, demanding two isolated same flavor leptons with  $p_T > 25, 20$  GeV, respectively,  $20 < m_{ll} < 70$  GeV, and at least two jets with  $p_T > 35$  GeV and pseudorapidity  $|\eta| < 2.5$  [3]. For two anti- $k_T$  jets of distance parameter  $R = 0.4$ , ATLAS requires  $\cancel{p}_T > 150$  GeV and for three or more,  $\cancel{p}_T > 100$  GeV. ATLAS observed 1133 events in this (‘SR-loose same-flavor combined’) signal region on an estimated background of  $1190 \pm 40 \pm 70$ , where the first quoted uncertainty is statistical and the second is systematic. Combining the two uncertainties in quadrature and profiling over an assumed Gaussian background expectation, we derive a 95% CL upper limit on the number of signal events in this signal region of 125.0.

Because the ATLAS cuts are slightly different to those of CMS, we must perform simulations in order to determine the ATLAS cut efficiencies and see whether the upper limit on the number of signal events constrains the parameter space significantly. Again our implementation of the analysis has been validated against ATLAS results. Figure 9 shows that the ATLAS search does constrain the part of golden-channel parameter space that fits the CMS  $lljj\cancel{p}_T$  analysis to 95% CL, but that there is still plenty of viable parameter space left. Most of the viable parameter space ruled out by the ATLAS off- $Z$  search is also already ruled out by the jets plus  $\cancel{p}_T$  search.

Since we have chosen the parameters of our signal model to yield high branching ratios of squarks to dileptons plus  $\cancel{p}_T$ , there is the possibility of both squarks decaying via the di-leptonic cascade. This then may pre-

<sup>6</sup> Feynman diagrams with gluinos in the  $t$ -channel contribute to

di-squark production.

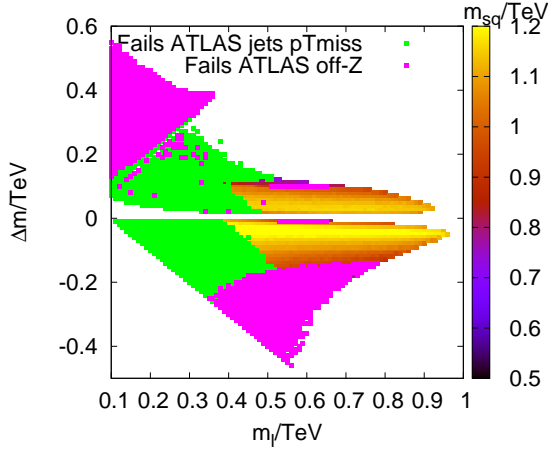


FIG. 9. Constraints on golden channel parameter space from the ATLAS  $lljj\cancel{p}_T$  on- $Z$  search. The squark mass consistent with the 95% CL lower bound on the CMS  $lljj\cancel{p}_T$  signal is given by reference to the scale on the right-hand side. Magenta points are ruled out by the ATLAS search at the 95% CL, whereas those coloured green are ruled out by ATLAS  $p_T$  plus jets searches at the 95% CL.

dict a non-zero signal rate for four-lepton  $\cancel{p}_T$  channels, which must be checked against experimental searches. CMS [20] placed bounds upon such channels by requiring at least two OSSF lepton pairs,  $\cancel{p}_T > 100$  GeV, and that neither pair is likely to come from a  $Z$ -boson, *i.e.* neither has  $75 < m_{ll}/\text{GeV} < 105$ . The sample is split into a high energy region where the total scalar sum of visible transverse momenta,  $H_T > 200$  GeV and a low energy region where  $H_T < 200$  GeV.

The most constraining signal region expected for our hypothesised signal is the high energy region with zero  $b$ - or  $\tau$ -tags in addition. In the high energy region, CMS observed zero events on a SM background expectation of  $0.01 \pm 0.01$ . We deduce a 95% CL upper bound on a putative signal contribution of 3.0. If a model point predicts an expected signal rate of larger than 3.0 events, we consider the point to be ruled out by these four-lepton searches. The resulting constraints on the viable parameter space are shown in Fig. 10. We see that the four-lepton search places strong constraints upon the model, ruling out nearly all of the remaining parameter space of the model except for a thin sliver at  $\Delta m \approx 120$  GeV and  $0.4 < m_{\tilde{l}}/\text{TeV} < 0.6$ . This small remaining sliver is where the branching ratio of the golden channel decay  $BR(\tilde{q}_L \rightarrow \chi_2^0 q \rightarrow \tilde{l}_R^\pm l^\mp q \rightarrow \chi_1^0 l^+ l^- q)$  is less than around 6%, resulting in lower four-lepton signal rates.

The most relevant other search to our golden channel interpretation of the CMS excess is one by ATLAS for direct stop pair production in final states with two leptons.<sup>7</sup> ATLAS searched in  $20.3 \text{ fb}^{-1}$  of integrated lu-

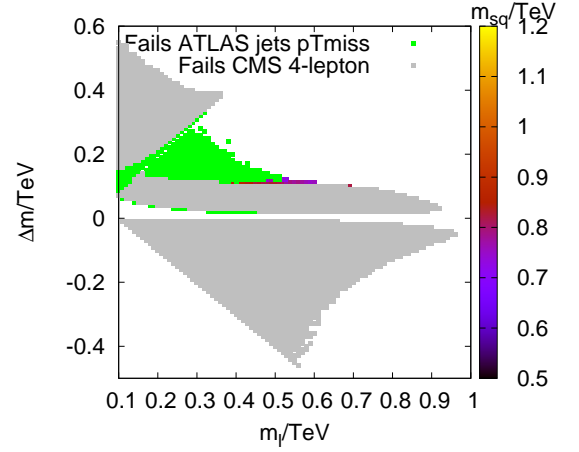


FIG. 10. Constraints on golden channel parameter space from the CMS  $4l\cancel{p}_T$  search. The squark mass consistent with the 95% CL lower bound on the CMS  $lljj\cancel{p}_T$  signal is given by reference to the scale on the right-hand side. Light gray points are ruled out by the CMS 4-lepton search at the 95% CL, whereas those coloured green are ruled out by ATLAS jets  $p_T$  searches, at the 95% CL.

minosity of 8 TeV  $pp$  collisions, in channels with exactly two oppositely charged leptons with  $p_T > 25, 20$  GeV, respectively, and  $m_{ll} > 20$  GeV. In the most sensitive signal region (L110), at least two anti- $k_T$  jets of distance parameter 0.4 were required to have  $p_T > 100, 50$  GeV, respectively. Cuts on the stransverse mass variable [22]  $m_{T2} > 110$  GeV, the azimuthal angle between the jets and the  $\cancel{p}_T$  vector,  $\Delta\phi_j > 1.0$ , and the azimuthal angle between the  $\cancel{p}_T$  and  $p_T = \cancel{p}_T + p_T(l_1) + p_T(l_2)$ ,  $\Delta\phi_l < 1.5$ , were also employed in order to increase the expected sensitivity over backgrounds.

ATLAS observe 3 events on a background of  $5.2 \pm 2.2$ , which they calculate corresponds to a 95% CL upper bound on a putative beyond the Standard Model contribution of 5.6 events. We show the effect on our parameter space in Fig. 11. Seven points are left after applying this constraint, each of which is excluded by the ATLAS jets plus  $\cancel{p}_T$  search.

As a check of the robustness of this result we have varied other parameters than the ones shown as axes in our figures one by one: we have increased the gluino mass to 2 TeV, we have changed the slepton mass ratio  $m_{\tilde{l}_L}(M_{SUSY})/m_{\tilde{l}_R}(M_{SUSY}) = 1.5, 2.5$ , completely decoupled the left-handed slepton  $m_{\tilde{l}_L}(M_{SUSY}) = 1$  TeV, split the squark masses  $m_{\tilde{q}_R}(M_{SUSY}) = m_{\tilde{q}}(M_{SUSY}) + 200$  GeV and  $m_{\tilde{q}_L}(M_{SUSY}) = m_{\tilde{q}}(M_{SUSY}) + 200$  GeV. However, the results are very similar to those shown above and the conclusion is identical in each case: the search for jets plus  $\cancel{p}_T$  and the stop pair search rule out

<sup>7</sup> The strong effect of this search was first pointed out by the au-

thors of [21]. We include it here for completeness following a revision of our original preprint.

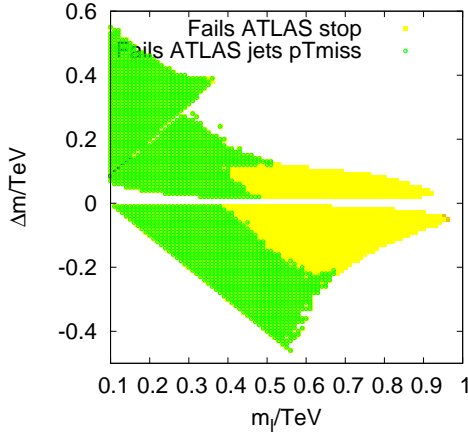


FIG. 11. Constraints on the golden channel parameter space from the ATLAS stop pair production search involving two leptons. Yellow points are ruled out by the ATLAS search for leptonically decaying stops at the 95% CL, whereas those coloured green are ruled out by ATLAS jets plus  $\cancel{p}_T$  searches at the 95% CL.

the whole of the parameter space that is consistent at 95% CL with the CMS  $jjll\cancel{p}_T$  excess.

## IV. CONCLUSIONS

To summarize, we have shown that a golden cascade interpretation of the CMS excess in  $lljj\cancel{p}_T$  events is apparently viable in its own terms. A recent ATLAS search using similar cuts leaves a sizeable portion of parameter space consistent with the  $lljj\cancel{p}_T$  excess at the 95% CL. However, the interpretation is in tension with other sparticle searches. In particular, the combination of ATLAS searches for jets plus  $\cancel{p}_T$ , an ATLAS di-stop search involving two leptons and a CMS four-leptons plus  $\cancel{p}_T$  search has no overlap at the 95% CL with the CMS excess.

## ACKNOWLEDGMENTS

This work has been partially supported by STFC grant ST/L000385/1. We thank the Cambridge SUSY Working Group and T. Stefaniak for stimulating discussions. Some of the CPU intensive parts of this work was performed on the Abel Cluster, owned by the University of Oslo and the Norwegian metacenter for High Performance Computing (NOTUR), and operated by the Research Computing Services group at USIT, the University of Oslo IT-department. The computing time was given by NOTUR allocation NN9284K, financed through the Research Council of Norway.

- 
- [1] *Search for physics beyond the standard model in events with two opposite-sign same-flavor leptons, jets, and missing transverse energy in pp collisions at  $\sqrt{s} = 8$  TeV*, Tech. Rep. CMS-PAS-SUS-12-019 (CERN, Geneva, 2014).
  - [2] V. Khachatryan *et al.* (CMS), *JHEP* **1504**, 124 (2015), [arXiv:1502.06031 \[hep-ex\]](#).
  - [3] G. Aad *et al.* (ATLAS), (2015), [arXiv:1503.03290 \[hep-ex\]](#).
  - [4] A. J. Barr and C. G. Lester, *J.Phys.* **G37**, 123001 (2010), [arXiv:1004.2732 \[hep-ph\]](#).
  - [5] D. Miller, P. Osland, and A. Raklev, *JHEP* **0603**, 034 (2006), [arXiv:hep-ph/0510356 \[hep-ph\]](#).
  - [6] C. Lester, M. A. Parker, and M. J. White, *JHEP* **0710**, 051 (2007), [arXiv:hep-ph/0609298 \[hep-ph\]](#).
  - [7] P. Huang and C. E. M. Wagner, *Phys.Rev.* **D91**, 015014 (2015), [arXiv:1410.4998 \[hep-ph\]](#).
  - [8] B. Allanach, C. Lester, M. A. Parker, and B. Webber, *JHEP* **0009**, 004 (2000), [arXiv:hep-ph/0007009 \[hep-ph\]](#).
  - [9] M. Cacciari, G. P. Salam, and G. Soyez, *JHEP* **0804**, 063 (2008), [arXiv:0802.1189 \[hep-ph\]](#).
  - [10] M. Cacciari, G. P. Salam, and G. Soyez, *Eur.Phys.J.* **C72**, 1896 (2012), [arXiv:1111.6097 \[hep-ph\]](#).
  - [11] B. Allanach, J. Conlon, and C. Lester, *Phys.Rev.* **D77**, 076006 (2008), [arXiv:0801.3666 \[hep-ph\]](#).
  - [12] P. Z. Skands, B. Allanach, H. Baer, C. Balazs, G. Belanger, *et al.*, *JHEP* **0407**, 036 (2004), [arXiv:hep-ph/0311123 \[hep-ph\]](#).
  - [13] B. Allanach, *Comput.Phys.Comm.* **143**, 305 (2002), [arXiv:hep-ph/0104145 \[hep-ph\]](#).
  - [14] A. Djouadi, M. Muhlleitner, and M. Spira, *Acta Phys.Polon.* **B38**, 635 (2007), [arXiv:hep-ph/0609292 \[hep-ph\]](#).
  - [15] W. Beenakker, R. Hopker, M. Spira, and P. Zerwas, *Nucl.Phys.* **B492**, 51 (1997), [arXiv:hep-ph/9610490 \[hep-ph\]](#).
  - [16] T. Sjostrand, S. Mrenna, and P. Z. Skands, *JHEP* **0605**, 026 (2006), [arXiv:hep-ph/0603175 \[hep-ph\]](#).
  - [17] T. Sjostrand, S. Mrenna, and P. Z. Skands, *Comput.Phys.Comm.* **178**, 852 (2008), [arXiv:0710.3820 \[hep-ph\]](#).
  - [18] G. Aad *et al.* (ATLAS Collaboration), (2014), [arXiv:1405.7875 \[hep-ex\]](#).
  - [19] S. Chatrchyan *et al.* (CMS Collaboration), *JHEP* **1406**, 055 (2014), [arXiv:1402.4770 \[hep-ex\]](#).
  - [20] S. Chatrchyan *et al.* (CMS), *Phys.Rev.* **D90**, 032006 (2014), [arXiv:1404.5801 \[hep-ex\]](#).
  - [21] P. Grothaus, S. P. Liew, and K. Sakurai, (2015), [arXiv:1502.05712 \[hep-ph\]](#).
  - [22] C. Lester and D. Summers, *Phys.Lett.* **B463**, 99 (1999), [arXiv:hep-ph/9906349 \[hep-ph\]](#).